Response of droplet parameters to liquid viscosity in the flow field of an air-blast sprayer

Xi'en Zhou[1], Bing Xiahou[2], Long Zhang[3], Daozong Sun[4,5,6], Xiuyun Xue[4,5,6], Qiufang Dai[4,5,6], Shuran Song[4,5,6*]

(1. *College of Engineering, South China Agricultural University, Guangzhou 510642, China*;
2. *General Affairs Department, South China Agricultural University, Guangzhou 510642, China*;
3. *Datang Hubei Energy Development Co., Ltd, Wuhan, 430000, China*;
4. *College of Electronic Engineering/College of Artificial Intelligence, South China Agricultural University, Guangzhou 510642, China*;
5. *Guangdong Engineering Research Center for Monitoring Agricultural Information, Guangzhou 510642, China*;
6. *Guangdong Laboratory for Lingnan Modern Agriculture, Guangzhou 510642, China*)

Abstract: The physical properties of sprayed droplets such as viscosity affect their deposition on the target. In order to understand the response characteristics of droplet parameters to the viscosity of a spray solution, a three-dimensional model of the external flow field of an air-blast sprayer based on computational fluid dynamics (CFD) was established according to the actual spray range and the sprayer duct structure. The change rules of droplet diameter and droplet density with distance under different viscosities of the spray solution in the flow field were obtained through numerical solution of the CFD model. The reliability of the model was verified by a chi-squared test comparing the numerical calculations with the results of field experiments. The results showed that the change rule of droplet parameters in an airflow field under different values of the spray solution viscosity was consistent. With the increase in the axial distance, the droplet size decreased initially, then increased, and finally decreased, while the droplet density gradually decreased. Moreover, the greater the spray solution viscosity, the shorter the conveying distance of the droplets in the axial direction, although viscosity was helpful in reducing the droplet drift. In addition, at the same axis distance, with the increased viscosity of the spray solution, the droplet size increased, and the sedimentation of the droplets was more rapid, while the density of the droplets decreased. The results provided a new framework for the study of air-blast spraying technology and serve as a reference for the optimization of the sprayer structure and the preparation method for spray solutions.

Keywords: air-blast sprayer, computational fluid dynamics, droplet diameter, droplet density, viscosity
DOI: 10.25165/j.ijabe.20231605.7380

Citation: Zhou X E, Xia H B, Zhang L, Sun D Z, Xue X Y, Dai Q F, et al. Response of droplet parameters to liquid viscosity in the flow field of an air-blast sprayer. Int J Agric & Biol Eng, 2023; 16(5): 28–34.

1 Introduction

As one of the main methods used to reduce crop pests and diseases, chemical control has received considerable attention. Foliar spraying is the most common method employed in chemical pest control. However, the efficiency of foliar spraying is easily reduced due to droplet drift and other factors. The drifting and lost pesticide particles not only cause significant waste but also affect human health and may pollute the environment. As an advanced foliar spraying technique[1], the air-blast spray technology has become increasingly attractive. Air-blast spray is a technology that uses high-speed airflow to send droplets to distant targets. Due to the target branches and leaves being affected by the airflow in the wind field, the fog droplets enter the outer layer and inner chamber of the fruit tree crown and attach to the upper and lower surfaces of the target crop leaves[2]. Therefore, the air-blast spray technology can effectively improve the utilization rate of pesticides[3] and reduce environmental pollution caused by drift[4].

Field experiments and CFD simulation are the two main methods used to improve the effect of air-blast spray. These include sprayer structure optimization and measurements of the sprayer airflow field, droplet parameters, and deposition rates.

In sprayer structure optimization, researchers have primarily focused on improving spray effectiveness by optimizing the structures of the sprayer duct, the deflector, and nozzles as well as by adding intelligent technology. Xu et al.[5] explored the influence of airflow velocity and installation angle of an air-blast sprayer on the airflow velocity field through CFD simulation and experiments; their results were applied to the structure of bellows. Fan et al.[6] proposed a directional target spraying machine with adjustable distance and controllable direction that could achieve accurate targeting according to spraying requirements. Qu et al.[7] improved

Received date: 2022-01-26 **Accepted date:** 2023-03-26
Biographies: Xi'en Zhou, PhD candidate, Intermediate Laboratory Technician, research interest: precision spraying technology. Email: season@scau.edu.cn; **Bing Xiahou**, MS, Engineer, research interest: agricultural engineering technology and precision spraying technology, Email: 346593633@qq.com; **Long Zhang**, MS, Engineer, research interest: air-assisted spraying, Email: 545692102@qq.com; **Daozong Sun**, PhD, Associate Professor, research interest: agricultural engineering application of embedded system and water-saving irrigation technology, Email: sundaozong@scau.edu.cn; **Xiuyun Xue**, PhD, Senior Laboratory Technician, research interest: agricultural engineering technology and precision spraying technology, Email: 59113829@qq.com; **Qiufang Dai**, PhD, Lecturer, research interests: spraying equipment and its key technology, Email: 149960069@qq.com.
***Corresponding author: Shuran Song**, Shuran Song, PhD, Professor, research interest: spraying technology and measurement and control technology. College of Electronic Engineering/College of Artificial Intelligence, South China Agricultural University, Guangzhou 510642, China. Tel: +86-13668966908, Email: songshuran@scau.edu.cn.

the design of the 3WZF-400A orchard air-blast sprayer through CFD by setting short diversion plates with different numbers and angles. Song et al.[8-11] developed and optimized the structure of the deflector and sprayer duct through CFD simulation of the internal flow field of an air-blast sprayer. Liu et al. installed a fluid guide at the outlet of a 9WZCD-25 air-blast sprayer that improved the uniformity and density distribution of droplets and partially increased the spraying area[12]. Li et al.[13,14] studied the droplet deposition characteristics of a self-made air-blast sprayer through CFD. In addition, some intelligent spray technologies have been used to improve the effect of air-blast sprayers, increase the pesticide droplet deposition rate, and reduce pesticide droplet drift.

Researchers have also obtained the general change rule of droplet parameters under different conditions by studying the airflow field, droplet parameters, and deposition rate in order to provide a reference for enhancing the deposition of the droplets. Xia et al.[15] established a CFD-based 3D model of an air-blast sprayer duct and the external airflow field to simulate droplet flow tracks, droplet flow parameters, and deposition. Kira et al.[16] measured and compared the vertical profile of spray drift generated by different sprayers and derived methods of reducing droplet drift. Song et al.[17,18] used an air-blast sprayer as a test platform, and the change rule of droplet size under different conditions was comparatively studied. Pergher et al.[19] used Fluent software to simulate the deposition distribution and anti-drift effect of droplets under different conditions for air-blast sprayers with a single sprinkler and established a droplet deposition distribution model. In order to study the effect of wind speed and direction on the spray airflow, Endalew et al.[20] presented a new CFD model for air-blast sprayers in orchards to predict the high and low distributions of spray airflow velocities in different canopy density areas and confirmed the inverse linear attenuation of the airflow. By establishing a CFD-based 3D model for droplet drift, Nuyttens et al.[21] verified the CFD model as an effective tool for reducing droplet drift; their model considered factors such as the characteristics of droplets, meteorological conditions, pesticide solution characteristics, canopy structure, and crop characteristics. Baetens et al.[22] simulated the droplet drift distribution of an air-blast sprayer and the effect of different factors on the deposition distribution of droplets. Panneton et al.[23] measured the effect of airflow velocity and flow on canopy penetration ability. Gu et al.[24] studied the effects of the speed of the spray fan, spray pressure, and spray distance on the distribution of droplets in the vertical direction and obtained regression equations for droplet distributions and working factors. Salcedo et al.[25,26] focused on the effects of sprayer airflow and its turbulence in the tree canopy and proposed a 2D CFD model of airflow generated by an axial fan air-blast sprayer in front of a citrus canopy that adopted a new turbulence model (SST K-ω) that could better simulate the real situation. In addition, researchers have also developed evaluation methods[27] and sensor systems[28] to examine the drift of droplets and to predict the deposition of droplets.

Previous researchers have focused on the structural optimization of an air-blast sprayer and its airflow field via droplet motion parameters but have focused less on the influence of the spray solution's physical properties on the droplet motion law and the changes in an airflow field. In this study, the general change rule of droplet size and density parameters in an airflow field under different values of the viscosity were obtained by numerical calculations using a model based on CFD. The results can provide references for the structural optimization of an air-blast sprayer and the preparation method for the spray solution.

2 Materials and methods

2.1 Selection of spray solution viscosity

This study was intended to investigate the effect of spray solution viscosity on the droplet parameters of an air-blast sprayer, and thus the choice of viscosity should be representative. Emulsion, wettable powder, suspending agents, and water dispersible granules are the common dosage forms for pesticides, and four representative pesticides, namely pyridaben, imidacloprid, spirodiclofen, and acetamiprid, were chosen to obtain viscosity test data.

The four pesticides were formulated into solutions according to the relevant instructions for dosage forms, and the ratios were 1:2200, 1:3400, 1:4000, and 1:25 000, respectively. Their viscosities were measured using an ndj-8t digital rotational viscometer produced by Shanghai Fangrui Instrument Co., Ltd. (the measurement range was 1-2 000 000 cp; the measurement error was ±1%, and the repetition error was ±0.5%.). Viscosity values were taken every 2 min for a total of three readings, and the average value of three readings was taken as the final viscosity value. The measured results were 1.25 cp, 1.50 cp, 1.64 cp, and 1.80 cp, respectively.

To improve the applicability of the model, the range of viscosity values adopted for numerical calculations needed to be further expanded on the basis of the range of viscosity values tested. Therefore, different viscosity values including 0.90 cp, 1.10 cp, 1.33 cp, 1.84 cp, and 2.20 cp were used in the numerical calculations. These values covered the range of viscosity for commonly used pesticide solutions, where 1.10 cp is the viscosity value of water. In the confirmatory field experiment, water was used as the spray solution to avoid pollution when spraying pesticides.

2.2 Numerical calculation method

In order to simulate the external airflow of an air-blast sprayer, the three-dimensional external airflow field model of the sprayer was established by ANSYS ICEM 17.0 and is shown in the dashed frame area in Figure 1.

Figure 1 External airflow field of the air-blast sprayer

2.2.1 3D model for the profile of the airflow field

According to previous research[2], the maximum horizontal spray range, vertical spray range, and axis direction distance of the air-blast sprayer used were 2.29 m, 2.52 m, and 12 m, respectively. As shown in Figure 2, the Cartesian coordinate frame was fixed at the center of the sprayer duct outlet as the origin O. The X-axis lies along the direction of the sprayer duct; the Y-axis is opposite to the gravity direction, and the XOY plane is the symmetrical plane. To ensure the accuracy of numerical calculation results and reduce the effect of boundary conditions on the airflow field, the model size was enlarged on the basis of the above spray range parameters. The width, height, and length of the 3D model of airflow field were set

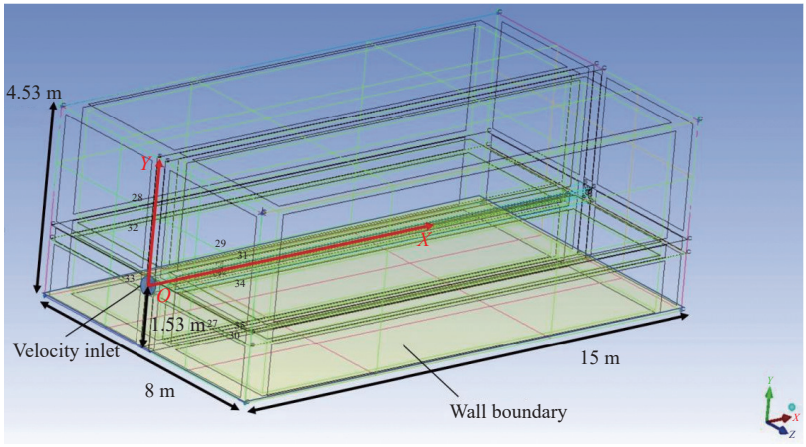

Figure 2 3D model for the external airflow field computational domain of an air-blast sprayer

as 8 m, 4.53 m, and 15 m, respectively. The distance of the sprayer duct outlet axis from the ground was 1.53 m.

2.2.2 Selection of the numerical calculation model

The object of the study was the droplet parameters in the external airflow field of an air-blast sprayer, including two-phase flow of air and droplets. Some physical factors such as gravity, inertia, droplet crushing and collision needed to be considered. Therefore, the discrete phase model (DPM) for the Euler–Lagrange method was used as the calculation model, as this was closer to the actual motion state of droplets in the flow field. The air was used as the continuous phase, and the droplets were considered as the discrete phase in the numerical calculations.

Fluent DPM considers the trajectory of discrete phase droplets by the Lagrange method. The action force balance equations[29] of droplets in a Cartesian coordinate system are shown in Equations (1)-(4):

$$\frac{du_p}{dt} = F_D\left(u-u_p\right) = \frac{g_y\left(\rho_p-\rho\right)}{\rho_p} + F_y \tag{1}$$

$$F_D = \frac{18\mu}{\rho_p d_p^2}\frac{C_D Re}{24} \tag{2}$$

$$Re = \frac{\rho d_p|u_p-u|}{u} \tag{3}$$

$$C_D = a_1 + \frac{a_2}{Re} + \frac{a_3}{Re^2} \tag{4}$$

where, u is the airflow velocity, m/s; u_p is the droplet velocity, m/s; μ is the airflow viscosity, Pa·s; ρ is the airflow density, kg/m^3; ρ_p is the droplet density, kg/m^3; d_p is the droplet diameter, m; R_e is the relative Reynolds number, a dimensionless parameter; C_D is the drag coefficient, a dimensionless parameter; g_y is the gravitational acceleration in y-direction, m/s^2; F_y is other action forces in direction y, N; α_1, α_2, and α_3 are constants.

When calculating the droplet flow trajectory, the gain and loss of heat, mass, and momentum on discrete phase droplets along the trajectory act on the continuous phase at the same time. The coupling effect of discrete phase and continuous phase should be considered in the calculation of continuous and discrete phases. The governing equations were derived alternately until the computational solutions converged to realize two-way coupling.

Variation of droplet momentum:

$$F = \sum\left(\frac{18\mu C_D Re}{\rho_p d_p^2 24}\left(u_p-u\right) + F_{other}\right)\dot{m}_p\Delta t \tag{5}$$

Variation of droplet heat:

$$H = \frac{\dot{m}_{p,0}}{m_{p,0}}\left[\left(m_{p_{in}}-m_{p_{out}}\right)\left[-H_{lat_{ref}}+H_{pyrol}\right] - m_{p_{out}}\int_{T_{ref}}^{T_{p_{out}}} c_{p_p}dT + m_{p_{in}}\int_{T_{ref}}^{T_{p_{in}}} c_{p_p}dT\right] \tag{6}$$

Variation of droplet mass:

$$M = \frac{m_{p_{in}}-m_{p_{out}}}{m_{p,0}}\dot{m}_{p,0} \tag{7}$$

where, $\dot{m}_p$ is the mass flow rate of the droplets, kg/s; Δt is the time step; F_{other} is the other interaction forces, N; $\dot{m}_{p,0}$ is the initial mass flow rate of the droplet injection, kg/s; $m_{p,0}$ is the initial mass of the droplet, kg; $m_{p_{in}}$ is the mass of the droplet on cell entry, kg; $m_{p_{out}}$ is the mass of the droplet on cell exit, kg; c_{p_p} is the heat capacity of the droplet, J/kg·K; H_{pyrol} is the heat of pyrolysis as volatiles are evolved, J/kg; $T_{p_{in}}$ is the temperature of the droplet on cell entry, K; $T_{p_{out}}$ is the temperature of the droplet on cell exit, K; T_{ref} is the reference temperature for enthalpy, K; $H_{lat_{ref}}$ is the latent heat at reference conditions, J/kg[30].

2.2.3 Meshing and condition setting

The external flow field calculation model of the air-blast sprayer was relatively regular, with the XOY plane as the symmetric plane and left and right symmetry. To consider the grid quality and computer memory resources, a hexahedral structured method in ICEM was used for grid generation, and the grid and time step independence checking calculations were carried out. The final number of grids was 1.33 million, and the time step was 0.01 s.

The boundary condition settings were adopted as follows. The outlet of the sprayer duct was set as the model velocity inlet (the blue area in Figure 2), and the velocity was 25.01 m/s[2]. The ground was set as the wall (the yellow area in Figure 2) with no slip conditions, no permeability, and a thermal insulation boundary layer. Other boundary conditions were set as the pressure outlet, where the pressure was the standard atmosphere pressure. The numerical calculations were performed using the standard turbulence model k-ε equation. The solution contents and methods are listed in Table 1, and the residual convergence criterion of 10^{-6} was set.

Table 1 Solution contents and methods

Solution content	Solution method
Pressure-velocity coupling equation	SIMPLE algorithm
Pressure equation	Standard interpolation format
Velocity gradient equation	Least squares cell-based
Remaining equations	Second-order upwind method

2.2.4 Implementation

The numerical calculations were performed using ANSYS Fluent 17.0 on the established model. The parameters for the sprayer numerical calculation were consistent with the true values, where the spray pressure was set at 1.80 MPa, the wind speed was 25.01 m/s, and the spray solution viscosity values were set at 0.90 cp, 1.10 cp, 1.33 cp, 1.84 cp and 2.20 cp. Using the Fluent software post-processing function to show nephograms of diameter and density of droplets corresponding to each viscosity value, the volume median diameter and density parameters of different distances in the axis direction were exported and plotted for analysis.

2.3 Field experiment

The field experiment scenario is shown in Figure 3. The density of the spray droplets in the axis direction was measured using a self-developed device with the following sampling point settings: in the sprayer axis direction, 1 m from the outlet was set as the first sampling position, and every 1 m was set as one sampling position, for a total of 12 sampling positions. The density of the spray droplets was measured three times at each sampling positions and averaged for the final measurement.

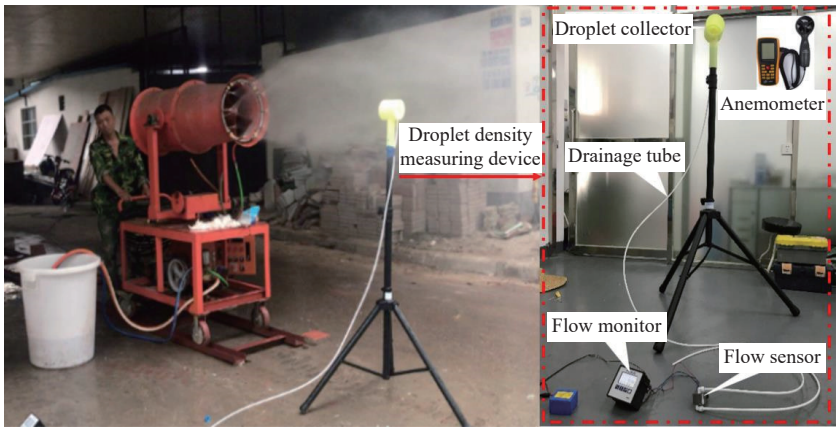

Figure 3 Experimental setup for droplet density measurement

Working principle of the droplet density measuring device: A droplet collector was placed in the flow field to accumulate the droplets in the axial direction when the air-blast sprayer was operating. The droplets were pooled into liquid and then passed through a drainage tube to the flow sensor. The sensor measured the flow value at the current position. The airflow anemometer measured the axial velocity at the same position. If the length and volume of the droplet collector were known, the droplet density at this position could be expressed by Equation (8). This value reflected the droplet distribution per unit volume in the spray area.

$$\varnothing = \frac{QL}{UV} \tag{8}$$

where, Q is the flow value, kg/s; L is the length of the droplet collector, m; U is the axial velocity, m/s; V is the volume of the droplet collector, m^3.

2.4 Verification

After the model was established, the reliability of the model was tested to verify the operation before it could be used to simulate field pesticide spraying. We focused on the droplet diameter and droplet density, and thus one of the two parameters was selected for field experiments when performing model validation. A significance test was applied to verify the reliability of the model based on the results of field experiments and numerical calculations under the same conditions. Because the droplet diameter was the integral distribution size over the accumulation of droplets (counting the proportion of droplets with less than a certain size), it was difficult to ensure the consistency of sampling between the numerical calculations and the field experiment. The droplet density was the mass of droplets in a unit volume measured by a self-made device, which could realize the consistency of sampling between the numerical calculations and the field experiment. Therefore, the droplet density was used as a parameter for model verification, and a chi-squared test was used to analyze the deviation between the actual observed value (field experiment results) and the theoretical inferred value (numerical calculation results).

3 Results and analysis

3.1 Numerical calculation

3.1.1 Effect of the spray viscosity on droplet diameter

The nephograms of droplet diameter at different viscosities are shown in Figure 4. Here, the nephograms are divided into two areas for comparison.

It can be seen from Zone 1 that when the viscosity of the spray solution was increased, the number of droplets and the droplet diameters also increased. According to Stokes' law[31], the droplets were subjected to gravitational, buoyant, and viscous forces in the y-axis direction:

$$v = \frac{2g_y\left(\rho_p - \rho\right)r^2}{9\mu}, \tag{9}$$

where, v is the settling speed of a droplet, m/s; r is the radius of a droplet, m.

According to Equation (9), the settling velocity of a droplet is proportional to the square of the droplet size. Therefore, the larger the droplet, the faster the sedimentation of the droplets. Specifically, in the range of 1.5-4 m, the droplets with large size settled rapidly. For example, when the viscosity was 2.20 cp, the droplets were relatively large, and they reached the floor at 1.5 m. At a lower spray solution viscosity such as 0.90 cp, the droplets were smaller in size and were transported 4.5 m before reaching the floor.

By comparing Zone 2 of each nephogram, it can be seen that when the spray solution viscosity was low, the drift phenomenon of the droplets was significant, and the droplets diffused and dispersed in this area. This increased the number of small-size droplets in this area. However, at higher viscosity the droplets became larger and settled without as much drift, indicating that increasing the viscosity of the spray solution would reduce the drift of the droplets.

Regarding the relationship between the variation of droplet size and the viscosity of the spray solution, Figure 5 shows that the

variation of droplet size along the axial direction under different spray solution viscosity. It is clear that under different values of spray solution viscosity, the volume median diameter of droplets with distance was basically consistent, decreasing initially, then increasing, and then gradually decreasing with the increase in the axial distance. In the range of 1-4 m, under the action of high-speed airflow the droplets were subject to air shear stress that changed large droplets to small droplets, and the volume median diameter of droplets gradually decreased. In the range of 4-9 m, the wind speed decayed with distance. The droplets aggregate and collide, changing from small droplets to large droplets, and the volume median diameter of droplets gradually increases. In the range of 9-12 m, it was the far part of the airflow field area that was less affected by wind speed. The possible reason for the smaller droplet size in this area was the drift and dispersion at the end of the airflow field, so the droplet size gradually decreased. In addition, due to the greater difficulty in spraying solutions with higher viscosity being atomized at the same axis distance, the droplet size was larger, and the volume median diameter of the droplets increased with the increase in viscosity.

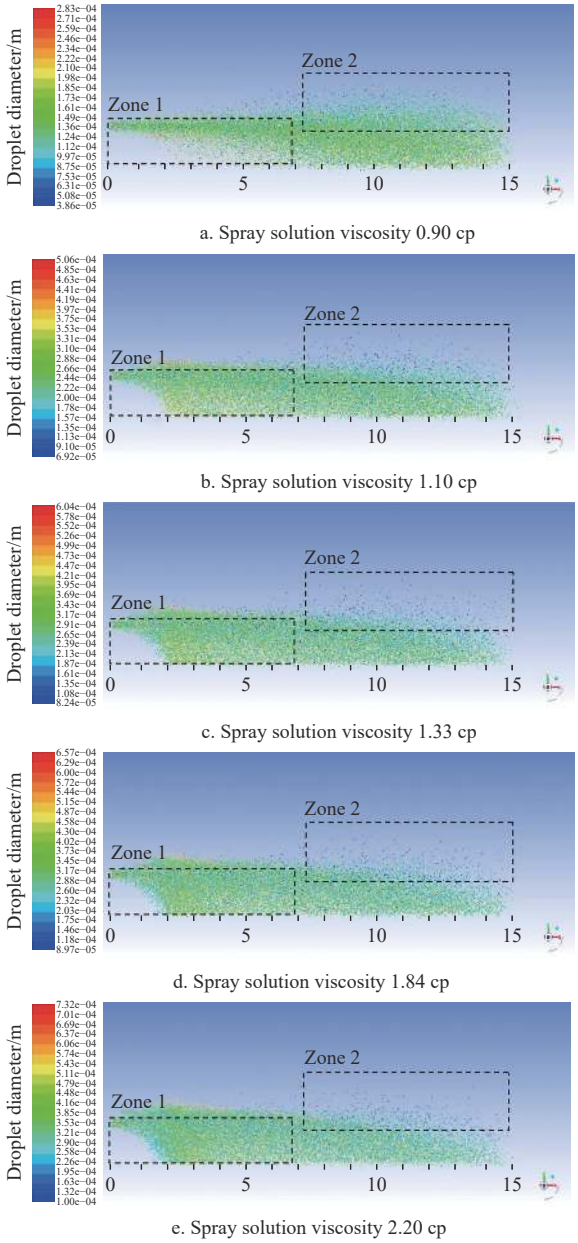

a. Spray solution viscosity 0.90 cp

b. Spray solution viscosity 1.10 cp

c. Spray solution viscosity 1.33 cp

d. Spray solution viscosity 1.84 cp

e. Spray solution viscosity 2.20 cp

Figure 4 Nephograms of droplet diameter at different viscosities

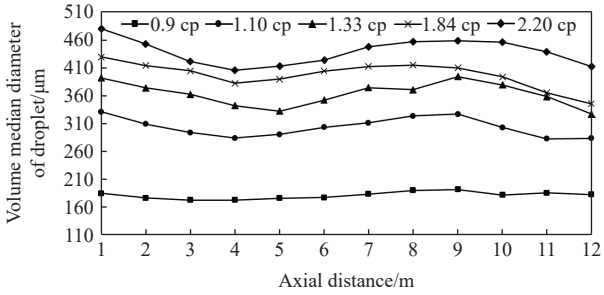

Figure 5 Variation curves for the volume median diameter of droplets

The study results were compared with those of other researchers[13,15,17]. Reference [15] studied the droplet flow characteristics and deposition in the airflow field of air-blast sprayer. It was found that droplet size had an effect on droplet settlement. The larger the droplet size, the higher the settling speed; small droplets can achieve a balance between gravity and air buoyancy, and thus can be transported further under the action of air flow. In [13], CFD technology was used to study the deposition characteristics of droplets in a self-made orchard air-blast sprayer. It was found that the drift of droplets increased with the distance from the nozzle. In [17], the authors studied the variation of droplet size in the airflow field of an air-blast sprayer. It was found that during the forward movement of droplets in the wind field, the droplet diameter decreased at first, then increased, and then again decreased. Although these studies did not consider the influence of droplet viscosity on droplet diameter, the results for the relationship between droplet size and the distance of the spray duct, the settling velocity, and drift were consistent with the results of our work.

3.1.2 Effect of the spray viscosity on droplet density

To study the influence of spray solution viscosity on the droplet density distribution of an air-blast sprayer, nephograms of droplet density distribution were drawn on the *XOY* axial plane at the outlet of the sprayer duct, as shown in Figure 6.

Figure 6 shows that the red colored part of region 1 decreased gradually when the viscosity changed from 0.90 cp to 2.20 cp, indicating that the density of the droplets decreased gradually in the axis direction when the viscosity of the spray solution increased. The reason was that when the viscosity of the spray solution became larger, the droplets were not as easily broken; there were fewer droplets, and thus the density of the droplets was lower. In addition, when the viscosity gradually increased, the spray distance decreased slightly. This was because when the viscosity increased, the droplet size became larger, and the large droplets were more influenced by gravity, resulting in a lower delivery capacity. Comparing each zone 2 of the nephograms, the droplets settled faster when the viscosity of the spray was higher.

Figure 7 shows the variation curves of droplet density at different viscosities. When the viscosity of the spray solution was varied, the overall change trend of droplet density with distance was basically the same, showing a gradually decreasing trend. The reason is that with the increase in the axial distance, the wind speed decreases; the transport capacity of the droplets decreases, and the drift of droplets increases. At the same axis distance, since the spray solution with lower viscosity is atomized more fully under the same wind speed, the droplets formed were denser, meaning that the density of droplets was higher. Similarly, under the same level of energy, the more viscous the spray solution, the less easy to atomize the solution into droplets. Therefore, the number of droplets was less, and thus the density of droplets was lower.

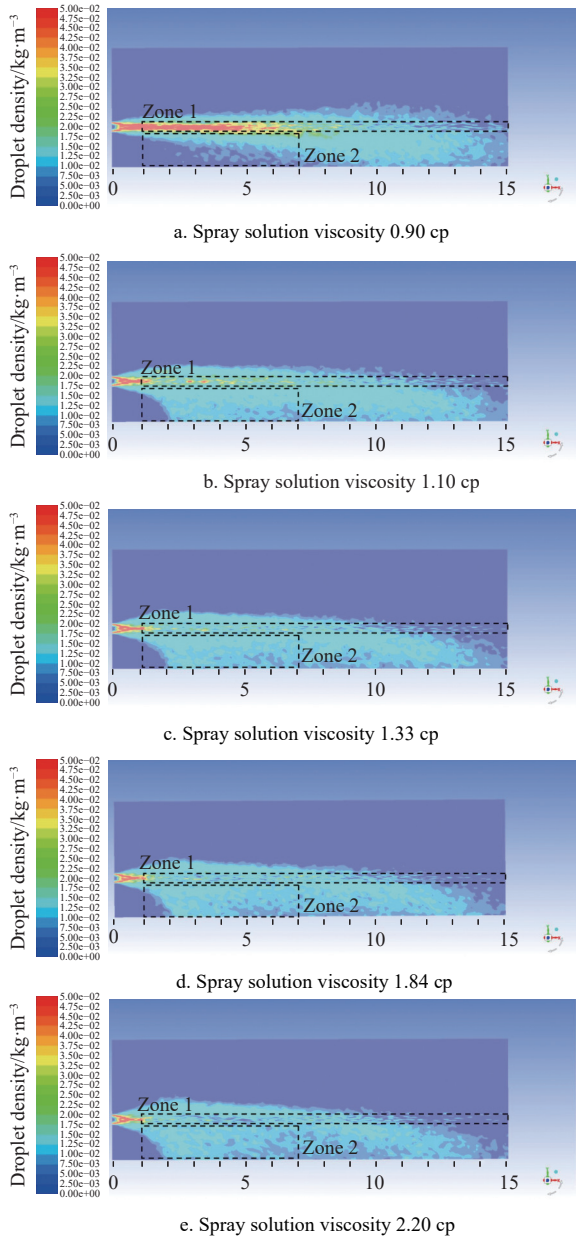

a. Spray solution viscosity 0.90 cp

b. Spray solution viscosity 1.10 cp

c. Spray solution viscosity 1.33 cp

d. Spray solution viscosity 1.84 cp

e. Spray solution viscosity 2.20 cp

Figure 6 Nephograms of droplet density distribution in the *XOY* axial plane

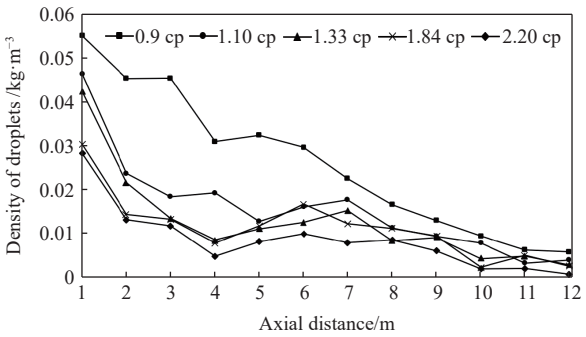

Figure 7 Variation curve for the droplet density at different viscosities

3.2 Model validation

Table 2 lists the model numerical calculation results and field experiment data for the droplet density at a spray solution viscosity of 1.10 cp.

A chi-squared test was used to determine whether there was a significant difference between the numerical calculations of the model and the data obtained from field experiment.

Table 2 Numerical calculation results and field experiment data for the droplet density

Axial distance /m	Droplet density/kg·m⁻³	
	1.10 cp	
	a	*b*
1	0.046 42	0.040 27
2	0.023 77	0.039 81
3	0.018 40	0.024 66
4	0.019 32	0.020 13
5	0.012 77	0.015 53
6	0.016 05	0.020 55
7	0.017 75	0.017 16
8	0.011 27	0.019 61
9	0.009 39	0.014 18
10	0.007 79	0.011 38
11	0.003 23	0.004 67
12	0.003 87	0.002 52

Note: *a* represents model numerical calculation results; *b* represents field experiment data.

The value of the test statistic X^2 was 0.027. For a significance level of 0.05 and 11 degrees of freedom, the critical value of the chi-squared distribution was 19.68. Therefore, the value of X^2 was much less than the critical value of the chi-squared distribution, indicating no significant difference between numerical calculation results and field experiment results for droplet density. This demonstrated that the established numerical calculation model for the sprayer external airflow field was reliable.

4 Conclusions

In this paper, the influence of spray solution viscosity on droplet size and droplet density in an airflow field was studied by CFD simulation. The conclusions drawn were as follows:

(1) Under different spray solution viscosities, the change rule of droplet parameters in an airflow field was consistent. As the axial distance increased, the droplet size decreased initially, then increased, and finally decreased, and the droplet density gradually decreased. The higher the spray solution viscosity, the shorter the conveying distance of the droplets in the axial direction, but the viscosity was helpful to reduce the drift of the droplets. Moreover, at the same axis distance, the increased viscosity of the spray solution made the spray droplet size larger; the sedimentation of the droplets was faster, and the density of the droplets was less.

(2) Through numerical calculations, the change rule of droplet size and droplet density with axis distance under different spray solution viscosities was obtained, and the results are significant for optimizing the sprayer structure parameters, reducing droplet drift, and reducing pesticide pollution in the environment. The chi-squared test indicated that the established model was effective and reliable. The model can also be used to study droplet parameters in an airflow field under different spray solution viscosities, instead of actual field experiments, to reduce test costs and shorten the test cycle.

Acknowledgements

The authors gratefully acknowledge the financial support provided by the National Natural Science Foundation of China (Grant No. 31671591), Guangdong Provincial Special Fund for

Modern Agriculture Industry Technology Innovation Teams (Grant No. 2021KJ108), Guangzhou Science and technology planning project (Grant No. 202002030245), Ministry of Finance and Ministry of Agriculture and Rural Affairs: Special Fund for Construction of Modern Agricultural Industry Technology System (Grant No. cars-26).

[References]

[1] Fu X M, Lv X L, Ding W M. Present situation and technical demand of orchard plant protection machinery in China. Xinjiang Agricultural Mechanization, 2011; 1: 61–63. (in Chinese)

[2] Chen J R, Song S R, Sun D Z, Hong T X, Zhang L. Test on airflow field and spray characteristics for long-range air-blast sprayer. Transactions of the CSAE, 2017; 33(24): 72–79. (in Chinese)

[3] Osterman A, Godeša T, Hočevar M, Širok B, Stopar M. Real-time positioning algorithm for variable-geometry air-assisted orchard sprayer. Computers and Electronics in Agriculture, 2013; 98: 175–182.

[4] Xie S H, Chen B Q, Lai C P, Zeng F L, Lai X H. Application of long-range air-blast sprayer in pest control of hilly orange orchard in South Jiangxi Province. South China Fruits, 2016; 45(1): 33–34+38. (in Chinese)

[5] Xu Y M, Zhu X W, Liu Z J, Hu Y H, Gu F. Field simulation and structure optimization of the air conveying system in air assisted sprayer based on computer fluid dynamics. Journal of Zhejiang University (Agric. & Life Sci.), 2018; 44(4): 451–458. (in Chinese)

[6] Fan G J, Wang Y Z, Zhang L, Yang Q L, Zhang X H, Wang Y. Design and experiment of caterpillar air-assisted orchard sprayer. Journal of Agricultural Mechanization Research, 2018; 40(5): 117–120. (in Chinese)

[7] Qu F, Sheng X Y, Li X, Zhang J X, Li W, Liu J Y. Improved Design of 3WZF-400A Orchard Air-assisted Sprayer. Transactions of the CSAM, 2017; 48(S1): 15–21. (in Chinese)

[8] Song S R, Xia H B, Lu Y H, Hong T S, Ruan Y C. Structural optimization and experiment on fluid director of air-assisted sprayer. Transactions of the CSAE, 2012; 28(6): 7–12. (in Chinese)

[9] Song S R, Xia H B, Liu H S, Hong T S, Sun D Z, Lu Y H. Numerical simulation and experiment of structural optimization for air blast sprayer. Transactions of the CSAM, 2013; 44(6): 73–78, 55. (in Chinese)

[10] Song S R, Ruan Y C, Hong T S, Dai Q F, Xiahou B. Optimal design and test on expanding duct of wide-swath air-blast sprayer. Transactions of the CSAE, 2013; 29(18): 34–42. (in Chinese)

[11] Song S R, Hong T S, Liu H S, Ruan Y C, Chen J Z. Law of spatial airflow velocity distribution for wide-swath air-blast sprayer. Transactions of the CSAE, 2013; 29(24): 17–24. (in Chinese)

[12] Liu Q, Fu Z T, Qi L J, Shi J X, Chen F. Characteristics optimization experiments of 9WZCD-25 air-blast and ultra-low volume sprayer. Transactions of the CSAM, 2005; 36(9): 44–47. (in Chinese)

[13] Li J, Zhao C Q, Li S J, Chen H, Ding S F. Droplet deposition characteristics of CFD based orchard air-driven sprayer. Journal of Huazhong Agricultural University, 2019; 38(6): 7. (in Chinese)

[14] Bian Y L, Li J P, Xue C L, Wang P F, Li X H. Analysis on status quo and prospects of intelligent development of air-feed sprayer in orchard. Journal of Northeast Agricultural University, 2019; 51(2): 86–94. (in Chinese)

[15] Xiahou B, Sun D Z, Song S R, Xue X Y, Dai Q F. Simulation and experimental research on droplet flow characteristics and deposition in airflow field. Int J Agric & Biol Eng, 2020; 13(6): 16–24.

[16] Kira O, Dubowski Y, Linker R. In-situ open path FTIR measurements of the vertical profile of spray drift from air-assisted sprayer. Biosystems Engineering, 2018; 169: 32–41.

[17] Song S R, Chen J Z, Hong T S, Xue X Y, Xiahou B, Song Y, Variation of droplet diameter in wind field for long range air-assisted sprayer. Transactions of the CSAE, 2017; 33(6): 59–66. (in Chinese)

[18] Xiahou B, Song S R, Sun D Z, Chen J Z, Dai Q F, Xue X Y. Effect of spraying pressure on droplet diameter of long-range and wide-swath air-blast sprayers. Journal of Henan Agricultural Sciences, 2019; 48(2): 7. (in Chineser)

[19] Pergher G, Gubiani R, Cividino S R S, Dell'Antonia D, Lagazio, C. Assessment of spray deposition and recycling rate in the vineyard from a new type of air-assisted tunnel sprayer. Crop Protection, 2013; 45: 6–14.

[20] Endalew A M, Debaer C, Rutten N, Vercammen, J, Delele M A, Ramon H, et al. Modelling pesticide flow and deposition from air-assisted orchard spraying in orchards: A new integrated CFD approach. Agricultural and Forest Meteorology, 2010; 150(10): 1383–1392.

[21] Nuyttens D, Baetens K, Schampheleire M D, Sonck B. Effect of nozzle type, size and pressure on spray droplet characteristics. Biosystems Engineering, 2007; 97(3): 333–345.

[22] Baetens K, Nuyttens D, Verboven P, Schampheleire M D, Nicolaï B, Ramon H. Predicting drift from field spraying by means of a 3D computational fluid dynamics model. Computers and Electronics in Agriculture, 2007; 56(2): 161–173.

[23] Panneton B, Lacasse B. Effect of air-assistance configuration on spray recovery and target coverage for a vineyard sprayer. Canadian Biosystems Engineering, 2004; 46(7): 213–218.

[24] Gu C C, Liu Z J, Pan G T, Pu Y J, Yang F Z. Optimization of working parameters for 3MGY-200 axial air-assisted sprayer in kiwifruit orchards. Int J Agric & Biol Eng, 2020; 13(2): 81–91.

[25] Salcedo R, Garcera C, Granell R, Molto E, Chueca P. Description of the airflow produced by an air-assisted sprayer during pesticide applications to citrus. Spanish Journal of Agricultural Research, 2015; 13(2): e0208.

[26] Salcedo R, Granell R, Palau G, Vallet A, Garcerá C, Chueca P, Moltó E. Design and validation of a 2D CFD model of the airflow produced by an air blast sprayer during pesticide treatments of citrus, Computers and Electronics in Agriculture, 2015; 116: 150–161.

[27] Grella M, Gil E, Balsari P, Marucco P, Gallart M. Advances in developing a new test method to assess spray drift potential from air blast sprayers. Spanish Journal of Agricultural Research, 2017; 15(3): e0207.

[28] Li L L, Zhang R R, Chen L P, Yi T C, Xu G, Xue D X, et al. Development of sensor system for real-time measurement of droplet deposition of agricultural sprayers. Int J Agric & Biol Eng, 2021; 14(5): 19–26.

[29] Zhu H J. Fluent 15.0 practical guidelines for flow field analysis. Posts and Telecommunications Press, 2015; 290p. (in Chinese)

[30] ANSYS Fluent. 14.0 theory guide. Canonsburg, PA: ANSYS, 2011.

[31] Zhang M Y, Jing S R, Li G J. Fluid dynamics of higher engineering. Higher Education Press, 2012; 532p. (in Chinese)